



Universality in the relaxation of spin helices under XXZ spin-chain dynamics

Vladislav Popkov ^{1,2} Marko Žnidarič¹ and Xin Zhang ³

¹*Faculty of Mathematics and Physics, University of Ljubljana, Jadranska 19, SI-1000 Ljubljana, Slovenia*

²*Department of Physics, University of Wuppertal, Gausstraße 20, 42119 Wuppertal, Germany*

³*Beijing National Laboratory for Condensed Matter Physics, Institute of Physics, Chinese Academy of Sciences, Beijing 100190, China*



(Received 28 March 2023; accepted 24 May 2023; published 12 June 2023)

We describe the dynamics of a transverse spin-helix state—a product state with spatially rotating magnetization—under XXZ spin chain evolution. Due to experimental relevance we especially focus on magnetization dynamics. At long times the $U(1)$ symmetry of the Hamiltonian is restored, leading to the decay of transverse magnetization, which can be described as an exponential decay of a spatially harmonic profile. We show that the dependence of the short- and intermediate-time decay timescale, which in principle depends on all different parameters, like the wave vector of the initial helix, the anisotropy, etc., can be described well by a single scaling function. We also briefly discuss the evolution of magnetization current.

DOI: [10.1103/PhysRevB.107.235408](https://doi.org/10.1103/PhysRevB.107.235408)

I. INTRODUCTION

New experimental techniques allow one to create novel quantum states with unusual properties. Among them, helices in Heisenberg magnets with a uniaxial anisotropy were produced and manipulated in cold-atom experiments [1–4]. The simplicity of creation and chiral properties of the quantum helices, their nontrivial topology, and large magnetization current makes quantum helices attractive for potential applications in spintronics and quantum computing. With the aid of two-dimensional helices one finds nonequilibrium universality features [5]. Using helicity degrees of freedom as qubits was recently discussed in [6]. The stability of one-dimensional (1D) helix states to external noise can exceed the stability of the ground states, as was argued in [7]. The helices can be prepared from most simple initial “vacuumlike” states by application of resonant fields [8] or by an adiabatic rotation [9]. Due to their simple structure, helices can be also maintained by dissipation; namely, they become dark states under properly chosen local dissipative protocol, affecting only boundary spins [10,11]. Finally, 1D helices have a nontrivial content in terms of quasiparticles: in the Bethe ansatz framework, helices are formed by exotic quasiparticles carrying zero energy and finite momentum, the so-called phantom Bethe excitations [12].

Our purpose is to set up a general theoretical framework for a problem, addressed in an experiment [2,4]. The problem is to describe the time evolution of helices with arbitrary wave vector under a XXZ spin- $\frac{1}{2}$ coherent dynamics characterized by z -axis anisotropy Δ . Note that, unlike the helices with modulation in the XZ plane discussed in [3,13,14], we treat transverse helices with modulation in the XY plane. These two helix types behave completely differently under the XXZ dynamics; in particular, transverse helices can be long-lived quantum states [2,15]. A central object of interest in experimental studies [2,4] is the decay rate of transverse helix amplitude which is calculated from raw data using some *ad hoc* or phenomenological fit function. Here we show that the problem exhibits scaling features leading to universal behavior of the decay rate. More specifically, we show that the rate

of change of the transverse amplitude $\gamma(Q, \Delta)$ of a helix with wave vector Q under the XXZ dynamics with anisotropy Δ exhibits self-similar scaling,

$$\frac{\gamma(Q, \Delta)}{\cos Q} = \gamma\left(0, \frac{\Delta}{\cos Q}\right), \quad (1)$$

valid for short-time and intermediate-time windows. The range of validity of Eq. (1) depends on system parameters. For $\Delta = 0$ (noninteracting fermions), the scaling (1) is exact, and moreover, we find multipoint correlations to satisfy their own scaling relations. For other regimes, we supply arguments that Eq. (1) holds at least up to times where the transverse spin-helix state (SHS) amplitude drops by a factor of 2, which is the most experimentally relevant time window. Note that the decay rate γ always depends on time via its definition. Here we accept definition (37) based on a threshold, in order to make direct comparison with experiment [2].

In the following, we set up the problem and derive conceptually important properties and symmetries. We find that two real functions (the amplitude and the phase) fully describe the temporal dynamics of one-point correlations, and investigate these functions numerically and analytically. In the free-fermion XX case we find remarkable scaling properties for all equal time observables. Then we treat the general XXZ case, and derive scaling relation (1) leading to data collapse of experimentally accessible quantity, a half-amplitude decay rate. We compare our findings with existing experimental data. At the end we discuss the evolution of the magnetization current and give verifiable quantitative predictions.

II. SETUP OF THE PROBLEM

We are interested in the temporal evolution of a 1D SHS,

$$|\Psi_{Q,\theta,\varphi}\rangle = \bigotimes_{n=0}^{N-1} \begin{pmatrix} e^{-i\frac{Qn+\varphi}{2}} \cos \frac{\theta}{2} \\ e^{i\frac{Qn+\varphi}{2}} \sin \frac{\theta}{2} \end{pmatrix}, \quad (2)$$

$$QN = 0 \pmod{2\pi}, \quad (3)$$

describing a helix spiral with period $2\pi/Q$ in lattice units, constant polar angle $0 \leq \theta \leq \pi$, and phase φ . In the following we also use a shorthand notation $|\Psi_Q\rangle \equiv |\Psi_{Q,\theta,\varphi}\rangle$ and, especially for a spatially homogeneous version of SHS ($Q = 0$), we use $|\Psi_0\rangle$:

$$|\Psi_0\rangle = \left(e^{-i\frac{\varphi}{2}} \cos \frac{\theta}{2} \right)^{\otimes N} \cdot \left(e^{i\frac{\varphi}{2}} \sin \frac{\theta}{2} \right)^{\otimes N}.$$

Chiral and homogeneous SHSs are related as $|\Psi_Q\rangle = U_Q |\Psi_0\rangle$ via the simple transform U_Q given in Eq. (10). SHS (2) evolves via coherent quantum dynamics described by the XXZ Hamiltonian with periodic boundary conditions,

$$H = \sum_{n=0}^{N-1} h_{n,n+1}, \quad N+n \equiv n, \quad (4)$$

$$h_{n,n+1} = \sigma_n^x \sigma_{n+1}^x + \sigma_n^y \sigma_{n+1}^y + \Delta (\sigma_n^z \sigma_{n+1}^z - I),$$

with z -axis exchange anisotropy Δ . Equation (3) provides commensurability of a SHS in a periodic system. The time evolution $e^{-iHt} |\Psi_{Q,\theta,\varphi}\rangle$ is characterized by expectation values of observables, denoted as

$$\langle A(H, t) \rangle_Q \equiv \langle \Psi_{Q,\theta,\varphi} | e^{iHt} A e^{-iHt} | \Psi_{Q,\theta,\varphi} \rangle \quad (5)$$

[explicit dependence on θ, φ is omitted from the left-hand side of Eq. (5) for brevity], where A is the operator of an observable. Further on, we also omit unnecessary variables in $\langle A(H, t) \rangle_Q$ and $|\Psi_{Q,\theta,\varphi}\rangle$ whenever it will not lead to misunderstanding (the omitted variable is the same for all terms in an equality).

The particularity of state (2) is its chirality, characterized by integer $QN/(2\pi)$, the winding number in the clockwise direction, and current of z magnetization,

$$\langle j^z(t=0) \rangle = 2 \sin^2 \theta \sin Q, \quad (6)$$

$$j^z = 2(\sigma_n^x \sigma_{n+1}^y - \sigma_n^y \sigma_{n+1}^x).$$

In addition, for $\cos Q = \Delta$, SHS (2) is an eigenvector of $H|_{\Delta=\cos Q}$ with eigenvalue zero [12,16], so time evolution (5) can be viewed as a result of a quench from $H|_{\Delta=\cos Q}$ to H with arbitrary anisotropy at time $t = 0$. Finally, the SHS can be prepared in experiments by manipulating homogeneously polarized equidistantly separated qubits with a magnetic field gradient [2].

Under standard assumptions (see Appendix A for details), one can assume that a $U(1)$ -invariant operator like H on an infinite lattice will impose $U(1)$ symmetry on any of its subsystem of finite size asymptotically in time, leading, specifically, to decay of transversal magnetization:

$$\lim_{t \rightarrow \infty} \lim_{N \rightarrow \infty} \langle \sigma_n^\pm(t) \rangle = 0, \quad \forall n, \quad (7)$$

where $\sigma_n^\pm = \frac{1}{2}(\sigma_n^x \pm i\sigma_n^y)$.

III. GENERAL PROPERTIES OF SHS OBSERVABLES UNDER XXZ EVOLUTION

Property I: Relation between spatially shifted observables. Let A_n and A_{n+1} be the same operator, shifted by one site (the

operator itself can act on an arbitrary number of sites). Then,

$$\langle A_{n+1} \rangle = \langle V_Q^\dagger A_n V_Q \rangle, \quad (8)$$

$$V_Q = \bigotimes_n e^{-i\frac{Q}{2}\sigma_n^z}.$$

For a proof, denote by T an operator of a shift by one lattice site to the right. Obviously, $[T, H] = [V_Q, H] = 0$. Using the easily verifiable relation

$$T |\Psi_Q\rangle = V_Q |\Psi_Q\rangle,$$

we obtain

$$\begin{aligned} \langle A_{n+1}(t) \rangle &= \langle \Psi_Q | T^\dagger e^{iHt} A_n e^{-iHt} T | \Psi_Q \rangle \\ &= \langle \Psi_Q | V_Q^\dagger e^{iHt} A_n e^{-iHt} V_Q | \Psi_Q \rangle \\ &= \langle \Psi_Q | e^{iHt} V_Q^\dagger A_n V_Q e^{-iHt} | \Psi_Q \rangle, \end{aligned}$$

i.e., Eq. (8). Iterating Eq. (8) k times we get $\langle A_{n+k} \rangle = \langle (V_Q^{-k} A_n V_Q^k) \rangle$ for an expectation value of an operator shifted by k lattice units.

Property II: Scaling relation between expectations calculated with homogeneous state $|\Psi_0\rangle$ and with chiral state $|\Psi_Q\rangle$. Let A be an arbitrary operator and let Q satisfy Eq. (3). Then,

$$\langle A(H, t) \rangle_Q = \langle A'(H', t) \rangle_0, \quad (9)$$

where

$$A' = U_Q^\dagger A U_Q, \quad U_Q = e^{-i\frac{Q}{2} \sum_{n=0}^{N-1} n \sigma_n^z}, \quad (10)$$

$$\begin{aligned} H' &= \cos Q \sum_{n=0}^{N-1} \left(\sigma_n^x \sigma_{n+1}^x + \sigma_n^y \sigma_{n+1}^y + \frac{\Delta}{\cos Q} (\sigma_n^z \sigma_{n+1}^z - I) \right) \\ &\quad + \frac{\sin Q}{2} J, \end{aligned} \quad (11)$$

$$J = 2 \sum_{n=0}^{N-1} (\sigma_n^x \sigma_{n+1}^y - \sigma_n^y \sigma_{n+1}^x). \quad (12)$$

For a proof, note that $|\Psi_Q\rangle = U_Q |\Psi_0\rangle$. Inserting unity $U_Q^\dagger U_Q = I$ in the proper places, we obtain

$$\langle A(H, t) \rangle_Q = \langle \Psi_0 | e^{iH't} A' e^{-iH't} | \Psi_0 \rangle = \langle A'(H', t) \rangle_0,$$

where $X' = U_Q^\dagger X U_Q$.

Each term $\sigma_n^\alpha \sigma_{n+1}^\alpha$ in H becomes $(\sigma_n^\alpha)' (\sigma_{n+1}^\alpha)'$ after the U_Q transformation. To simplify further, we use easily verifiable relations:

$$(\sigma_n^x)' = \cos(nQ) \sigma_n^x - \sin(nQ) \sigma_n^y, \quad (13)$$

$$(\sigma_n^y)' = \cos(nQ) \sigma_n^y + \sin(nQ) \sigma_n^x, \quad (14)$$

$$(\sigma_n^z)' = \sigma_n^z. \quad (15)$$

Inserting the above into H' and using trigonometric identities we get Eq. (11).

In the thermodynamic limit $N \rightarrow \infty$, Q is arbitrary. Then, Eq. (9) allows to reduce a problem of SHS evolution with arbitrary wavelength Q to evolution of a homogeneous state $Q = 0$, under the transformed Hamiltonian H' , containing an additional Dzyaloshinskii-Moriya term [17,18], proportional to the total current of magnetization, J (12).

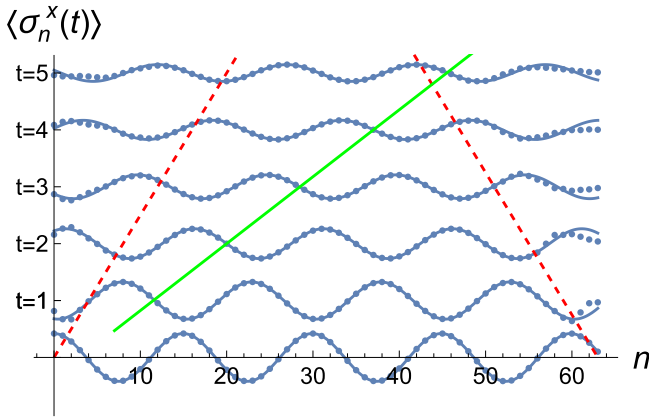


FIG. 1. Decaying traveling wave: x component of the magnetization profile at equal time intervals versus site number, for $\theta = \pi/5$, $Q = 0.42$, $\Delta = 0$. Magnetization profiles at different times $t = 0, 1, \dots, 5$ are shown with additional offsets for better visibility. Points are TEBD numerics for a chain with 64 sites and open boundary conditions, while interpolating harmonic curves are given by Eq. (20). Open boundary conditions generate perturbations at the edges, propagating in the bulk with the velocity $v_{\text{prop}} \approx 4$ per unit time (red dashed lines). The green line shows the location of the constant phase and is given by $n = vt + a$ where $v \approx 8.5$ per unit time.

In the following, we apply Properties 1 and 2 to study one-point observables, i.e., spin-helix magnetization profile, and selected two-point observable, the current of magnetization.

IV. DECAY OF TRANSVERSAL SHS COMPONENTS

The magnetization profile of SHS (2) at $t = 0$ is harmonic in space,

$$\frac{\langle \sigma_n^x(0) \rangle}{\sin \theta} = \cos(Qn + \varphi), \quad (16)$$

$$\frac{\langle \sigma_n^y(0) \rangle}{\sin \theta} = \sin(Qn + \varphi), \quad (17)$$

where θ is the polar angle and φ is the overall phase shift. Applying Eq. (8) with $A_n = \sigma_n^\alpha$ and using $e^{i\frac{Q}{2}\sigma^z} \sigma^\pm e^{-i\frac{Q}{2}\sigma^z} = e^{\pm iQ} \sigma^\pm$, and $e^{i\frac{Q}{2}\sigma^z} \sigma^z e^{-i\frac{Q}{2}\sigma^z} = \sigma^z$, we obtain

$$\langle \sigma_{n+1}^\pm(t) \rangle = e^{\pm iQ} \langle \sigma_n^\pm(t) \rangle, \quad (18)$$

$$\langle \sigma_{n+1}^z(t) \rangle = \langle \sigma_n^z(t) \rangle. \quad (19)$$

Equation (18) entails that the magnetization profile of the SHS stays strictly harmonic in space at all times t (see Fig. 1 for an illustration) and can therefore be described via a rescaled amplitude $S_N(t) \equiv S_N(Q, \theta, \Delta, t)$ and a phase shift $\phi(t) \equiv \phi(Q, \theta, \Delta, t)$, as

$$\frac{\langle \sigma_n^x(t) \rangle}{\sin \theta} = S_N(t) \cos(Qn + \varphi - \phi(t)), \quad (20)$$

$$\frac{\langle \sigma_n^y(t) \rangle}{\sin \theta} = S_N(t) \sin(Qn + \varphi - \phi(t)), \quad (21)$$

$$\begin{aligned} \langle \sigma_n^z(t) \rangle &= \cos \theta, \\ S_N(0) &= 1, \quad \phi(0) = 0. \end{aligned} \quad (22)$$

Here, Eq. (22) follows from Eq. (19) and the fact that the XXZ dynamics conserves total z magnetization.

Both S_N and ϕ depend not only on time and system size N but also on Q , θ , and Δ , while there is no dependence on the overall phase φ for obvious physical reasons. $S_N(t)$ and $\phi(t)$ satisfy the relations

$$S_N(t) = S_N(-t), \quad \phi(t) = -\phi(-t), \quad (23)$$

$$S_N(Q, \theta) = S_N(-Q, \theta) = S_N(Q, \pi - \theta),$$

$$S_N(Q, \Delta) = S_N(\pi - Q, -\Delta) \text{ for even } N,$$

$$\phi(\pi - \theta) = -\phi(\theta), \quad (24)$$

$$\phi(Q) = \phi(-Q)$$

(omitted parameters are the same on both sides), imposed by symmetries of the Hamiltonian and the SHS (see Appendix B). In particular it follows from Eq. (24) that

$$\phi(\theta, t)|_{\theta=\pi/2} = 0, \quad (25)$$

i.e., decay of the fully transversal SHS (the SHS with polarization lying in the XY plane) is described by just one function $S_N(t)$ in Eqs. (20) and (21). For $\theta \neq \pi/2$, and $|\Delta| < 1$, $\phi(t)$ quickly converges to $\phi(t) = vt$, which allows to view the magnetization profile as a traveling wave (see green line in Fig. 1). Further details about the phase are given in Sec. VIII. Note that the amplitude $S_N(t)$ can be easily measured experimentally while the phase is usually unknown.

We obtained explicit analytic form of $S_N(t)$ in several cases: for $|\Delta| \rightarrow \infty$ [see Eq. (36)], for $\theta \rightarrow 0$ (see Appendix D), and for the free-fermion case $\Delta = 0$, via an explicit determinantal representation [Eq. (28)].

Further, we are interested in thermodynamic limit $S_N(t)|_{N \rightarrow \infty} \rightarrow S(t)$, since it is an experimentally measurable quantity [2]. From Eq. (7) we expect the asymptotic decay of $S(t) \rightarrow 0$ at large times for any choice of parameters, apart from the case when the SHS is an eigenstate of H , i.e., for $\cos Q = \Delta$. We can determine early time behavior of $S(t)$ or any other observable via exact Taylor expansion [see Eqs. (34) and (39)].

To obtain the observables at intermediate times $t = O(1)$ we use time-evolving block decimation (TEBD) calculations (see Appendix G). The raw TEBD data are illustrated in Fig. 1. We use the central area near the middle site $n = N/2$ for all measurements, in order to avoid an influence of the borders. The data thus obtained effectively coincide with those from an infinite system. The quality of the TEBD data for the bulk can be checked by monitoring deviations for bulk integrals of motion. For instance, the $\langle \sigma_n^z \rangle$ component of the magnetization in the bulk must stay constant in space and time [see Eq. (22)]. Thus, we trust the density matrix renormalization group data for $S(t)$ up to the times when $\langle \sigma_n^z(t) \rangle - \langle \sigma_n^z(0) \rangle$ deviations start to appear in the middle of the chain, where we do the measurements. For the bond size $\chi = 20$ this leads to parameter-dependent t_{max} , the typical value being $t_{\text{max}} \approx 3$, which is enough for our purposes (see Appendix G for more details). In addition, we checked the TEBD correctness directly by comparison with the exact result of Eq. (28).

The case $\Delta = 0$ is special and deserves separate discussion.

V. XX CASE: SCALING FORM OF CORRELATIONS FOR DIFFERENT SHS WAVELENGTHS

For the free-fermion case $H \equiv H_{XX} = \sum_n (\sigma_n^x \sigma_{n+1}^x + \sigma_n^y \sigma_{n+1}^y)$, the total magnetization current J from Eq. (12) is a constant of motion: $[H_{XX}, J] = 0$. This renders the Dzyaloshinskii-Moriya term containing J in Eq. (11) irrelevant, if the initial state is an eigenstate of J . Indeed, in our case one can obtain $J |\Psi_0\rangle = 0$ (no gradient, no current), resulting in $e^{-iH_{XX}t} |\Psi_0\rangle = e^{-iH_{XX}t \cos Q} |\Psi_0\rangle$. Consequently, for $H \equiv H_{XX}$ the scaling property (9) simplifies as

$$\langle A(H_{XX}, t) \rangle_Q = \langle A'(H_{XX}, t \cos Q) \rangle_0. \quad (26)$$

An immediate consequence of Eq. (26) is a scaling relation for the SHS amplitude,

$$S_N(Q, t) = S_N(0, t \cos Q), \quad (27)$$

i.e., the curves $S_N(t)$ for different Q differ just by rescaling of time. Note that Eq. (27) is valid for any finite N , provided commensurability of Q [Eq. (3)].

$$S_4(t) = \frac{1}{8}(2 \cos(4t) + (3 + 2\sqrt{2}) \cos(4(\sqrt{2} - 1)t) + (3 - 2\sqrt{2}) \cos(4(1 + \sqrt{2})t)),$$

$$S_6(t) = \frac{1}{96}(8 \cos(4t) + 2 \cos(8t) + 4 \cos(4\sqrt{3}t) + (26 + 15\sqrt{3}) \cos(4(\sqrt{3} - 2)t)$$

$$+ 2(7 + 4\sqrt{3}) \cos(4(\sqrt{3} - 1)t) + 2(7 - 4\sqrt{3}) \cos(4(1 + \sqrt{3})t) + (26 - 15\sqrt{3}) \cos(4(2 + \sqrt{3})t) + 2).$$

For sufficiently large N , S_N from Eq. (28) gives an excellent approximation for $S(t)$ up to times when $S(t)$ becomes vanishingly small (see Fig. 2). The number of terms in S_N [Eq. (28)] grows exponentially with N .

Equation (27) allows to study just the homogeneous case $Q = 0$ without losing generality. The curves $S(t)$ for $Q = 0$ and different θ , obtained via TEBD, are given in Fig. 3. We see that the decay rate decreases with θ .

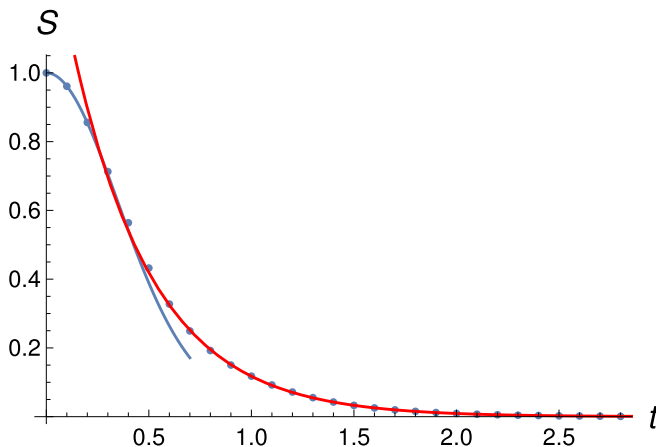


FIG. 2. Decay of the amplitude $S(t)$ for homogeneous initial state $|\Psi_0\rangle$, with $\theta = \pi/2$ under XX dynamics ($\Delta = 0$). Points stem from exact formula (28) for $N = 22$ sites. Interpolating red curve is given by $1.49e^{-2.54t}$. Interpolating blue curve is given by renormalized symmetric α -stable Lévy distribution [20] with $\alpha = 1.8$.

For even N and $\Delta = 0$, one finds [19] explicit expressions of $S_N(t)$ for $\theta = \pi/2$ and $Q = 0$:

$$S_N(t) = \frac{1}{N^N} \sum_{\mathbf{p}, \mathbf{q}} \cos(E_{\mathbf{p}, \mathbf{q}} t) \det G(\mathbf{p}) \det G(-\mathbf{q}) \times \det F(\mathbf{p}, \mathbf{q}),$$

$$F_{nm}(\mathbf{p}, \mathbf{q}) = \frac{1}{e^{i(p_n - q_m)} - 1}, \quad n, m = 1, 2, \dots, N/2, \quad (28)$$

$$G_{nm}(\mathbf{p}) = e^{2in p_m} (1 + e^{-i p_m}),$$

$$E_{\mathbf{p}, \mathbf{q}} = 4 \sum_{j=1}^{N/2} (\cos p_j - \cos q_j),$$

where F, G are $\frac{N}{2} \times \frac{N}{2}$ matrices and $\mathbf{p} \equiv \{p_1, p_2, \dots, p_{N/2}\}$, $\mathbf{q} \equiv \{q_1, q_2, \dots, q_{N/2}\}$, with p_k, q_k all different and satisfying $e^{ip_k N} = 1$, $e^{iq_k N} = -1$ (see [19] for details). For $N = 4, 6$, Eq. (28) gives

For the two-point correlations $S_{n,m}^{\alpha\beta}(Q, t) = \langle \sigma_n^\alpha \sigma_m^\beta(H_{XX}, t) \rangle_Q$, we get, for the simplest case $n = 0$ using Eq. (26),

$$S_{0,m}^{\alpha\pm}(Q, t) = e^{\pm imQ} S_{0,m}^{\alpha\pm}(0, t \cos Q), \quad (29)$$

$$S_{0,m}^{\alpha z}(Q, t) = S_{0,m}^{\alpha z}(0, t \cos Q). \quad (30)$$

For general n, m the scaling relations can be obtained from Eqs. (29) and (30) using Eq. (8). Generalization to the multi-point correlations is straightforward.

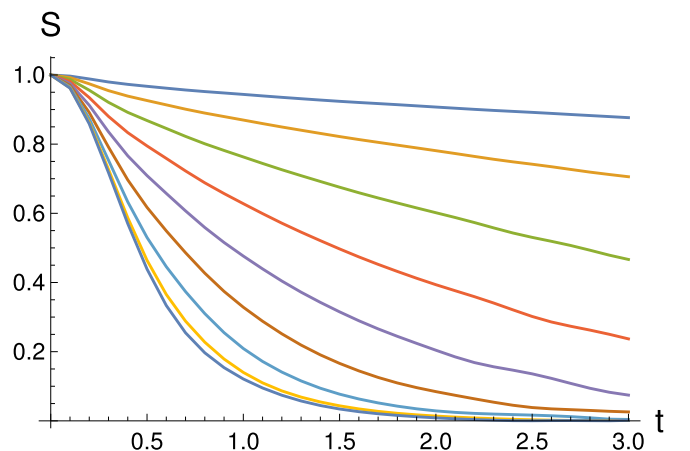


FIG. 3. Decay in time of the rescaled amplitude $S(t)$ of homogeneous SHS $|\Psi_0\rangle$, obtained from the TEBD calculations for $N = 64$, $\Delta = 0$, and different θ . Curves from top to bottom correspond to increasing θ values of $\theta/\pi = 0.1, 0.15, 0.2, \dots, 0.5$.

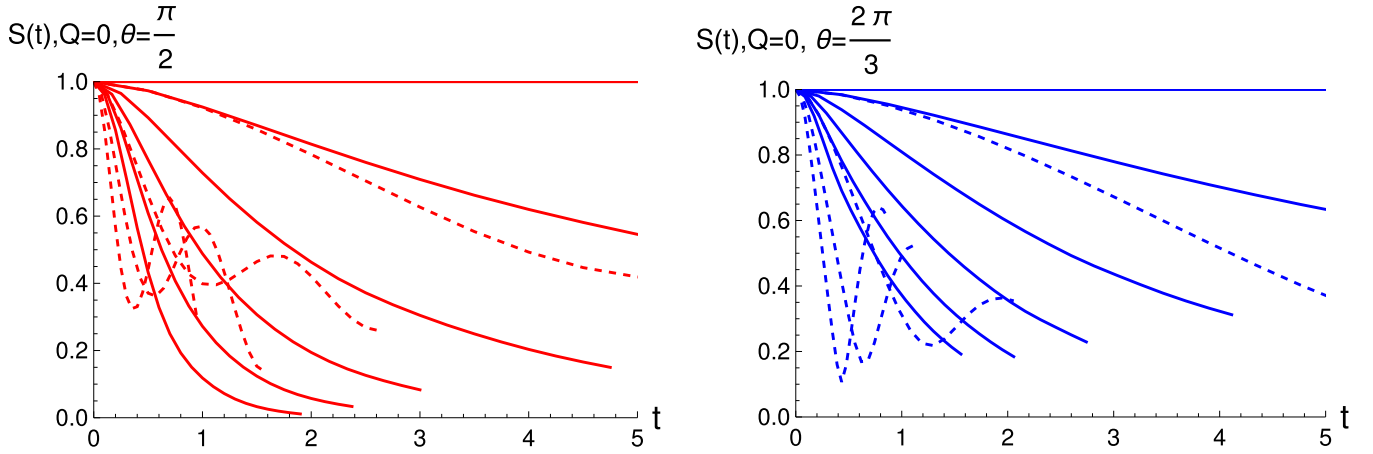


FIG. 4. Rescaled SHS amplitude $S(t)$ for $Q = 0$ for different Δ , for $\theta = \pi/2$ (left) and $\theta = 2\pi/3$ (right), from TEBD for open XXZ spin-1/2 chain with 64 sites. Full curves correspond to $|\Delta| \leq 1$, namely, $\Delta = 1, 0.8, 0.6, 0.4, 0.2, 0$ (from top to bottom). Dashed curves correspond to $\Delta > 1$, namely, $\Delta = 1.2, 1.8, 2.4, 3$; the shorter curves (i.e., those with smaller maximal value of t shown) correspond to larger Δ . The largest reported time for each dashed curve is given by $3 t_{\text{char}}$ from Eq. (35).

VI. XXZ CASE (ARBITRARY Δ)

For $\Delta \neq 0$ we find the early time evolution of observables using the expansion

$$e^X A e^{-X} = A + [X, A] + \frac{1}{2!} [X, [X, A]] + \dots = \sum_{n=0}^{\infty} \frac{1}{n!} \text{ad}_X^n(A), \quad (31)$$

$$\text{ad}_X(A) = [X, A], \quad \text{ad}_X^0(A) = A,$$

with X substituted by iHt and A being the operator of a chosen observable. For the expectation values, Eq. (31) yields

$$\langle A(t) \rangle = \langle A(0) \rangle + \sum_{k>0} C_k t^k, \quad (32)$$

valid for the thermodynamic limit $N \rightarrow \infty$ (see Appendix F for details). Generically, a characteristic timescale at which $\langle A(t) \rangle$ changes significantly can be estimated as

$$t_{\text{char}} = \left| \frac{C_{k_s}}{\langle A(0) \rangle} \right|^{\frac{1}{k_s}}, \quad (33)$$

where C_{k_s} is the first nonvanishing coefficient in Eq. (32). For the rescaled SHS amplitude, we obtain

$$\begin{aligned} S(t) &= 1 - 4t^2(\Delta - \cos Q)^2 \sin^2 \theta + O(t^4) \\ &= 1 - \left(\frac{t}{t_{\text{char}}} \right)^2 + O(t^4), \end{aligned} \quad (34)$$

$$t_{\text{char}} = |2(\Delta - \cos Q) \sin \theta|^{-1}. \quad (35)$$

So, $S(t)$ initially decreases with time, thus driving the one-site density matrix towards the $U(1)$ -symmetric point $S = 0$. The states with larger initial amplitude (larger $\sin \theta$) decay faster. The amplitude expansion (34) for $\Delta = 0$ up to the order t^{12} is given in Appendix F.

Another important feature of Eq. (35) is the divergence of t_{char} for $\Delta \rightarrow \cos Q$. Indeed for $\cos Q = \Delta$ the SHS $|\Psi_{Q,\theta,\varphi}\rangle$ becomes an XXZ eigenstate [12], leading to the time-independent SHS amplitude, and $t_{\text{char}} \rightarrow \infty$. To obtain $S(t)$ for intermediate times $t = O(1)$ and arbitrary Δ we use

TEBD. Figure 4 shows the rescaled amplitude $S(t)$ for $Q = 0$ and different values of Δ and θ .

We observe the onset of oscillations of $S(t)$ for $\Delta > 1$ (dashed curves in Fig. 4) with slower overall decay of the oscillation envelope. The emergence of the oscillations can be understood by considering the $\Delta \gg 1$ limit, which yields an oscillatory solution for $S(t)$ (see Appendix E):

$$S(t)|_{\Delta \gg 1} = \frac{1 + \cos^2 \theta}{2} + \frac{1}{2} \sin^2 \theta \cos(4(\Delta - a)t), \quad (36)$$

where the nonuniversal shift $a = O(1)$ results from $1/\Delta$ corrections. In addition, the presence of hopping terms [neglected in the derivation of Eq. (36)] leads to overall decay of the oscillation envelope with time, well visible in the TEBD data for $\Delta \gg 1$ (see Fig. 5).

Following [2], we characterize the SHS decay $S(t)$ by a parameter γ , the inverse time of the amplitude decay by one-

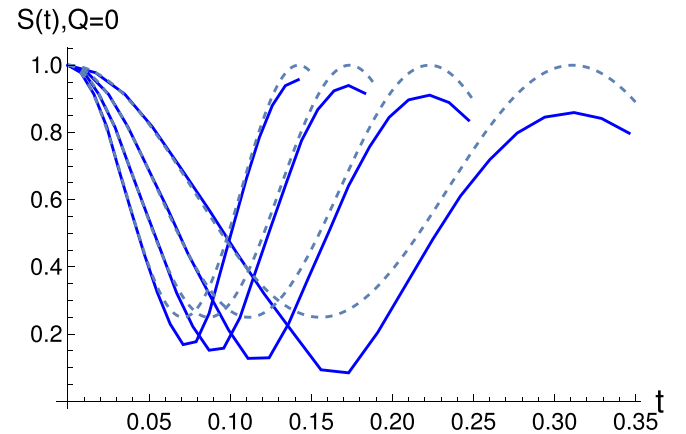


FIG. 5. Rescaled SHS amplitude $S(t)$ for $Q = 0$ for large Δ , for $\theta = 2\pi/3$ from TEBD. Solid curves connecting data points correspond to $\Delta = 6, 8, 10, 12$, while dashed curves show theoretical $\Delta \gg 1$ expressions (36) with fitted nonuniversal shift $a = 0.9$. Shorter curves correspond to larger Δ .

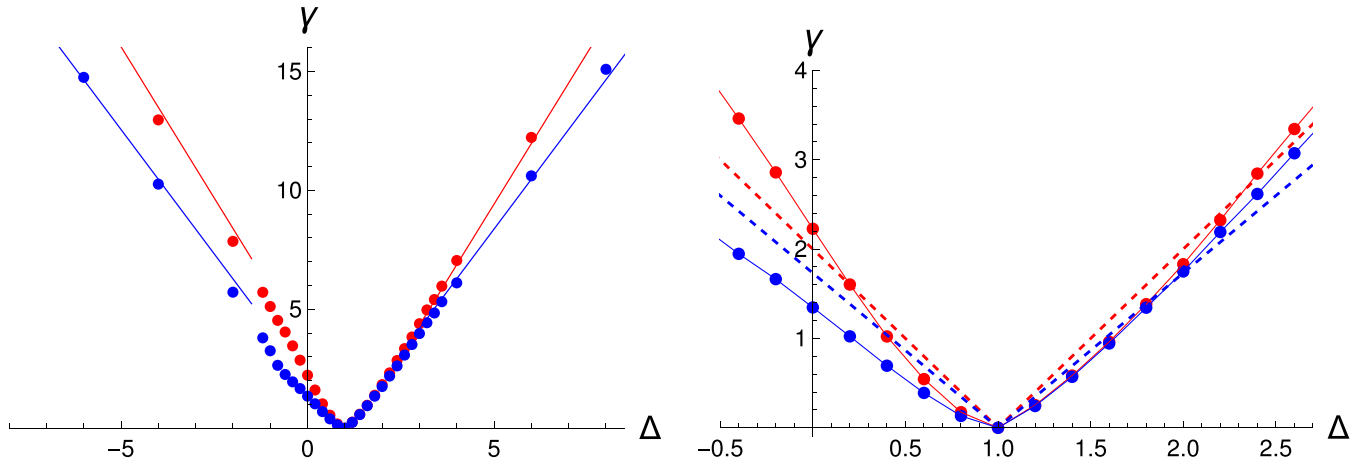


FIG. 6. Half-amplitude decay rate γ versus Δ for $Q = 0$ and $\theta = \pi/2$ (red data set), $\theta = 2\pi/3$ (lower blue data set), calculated from the data similar to the ones shown in Fig. 4, respecting the color code. Left: Solid straight lines have slopes, predicted from Eq. (38) for the $\Delta \rightarrow \infty$ limit. Right: Close-up view of left panel. Dashed straight lines show $\tau_{\text{char}}^{-1} = 2|\Delta - 1| \sin \theta$ for $\theta = \pi/2$ (red), $\theta = 2\pi/3$ (blue).

half,

$$S(1/\gamma) = \frac{S(0)}{2} = \frac{1}{2}. \quad (37)$$

A rough estimate for γ is given by the quantity $1/t_{\text{char}}$ in Eq. (35). For monotonic $S(t)$ dependence as in Fig. 3, γ has the meaning of a decay rate of the amplitude, while for $\Delta \gg 1$ when Eq. (36) is approximately valid, γ gives a measure for the rate of the amplitude change.

Note that the asymptotic $\Delta \rightarrow \infty$ values of $S(t)$ [Eq. (36)] obey $S(t) \geq \cos^2 \theta$. Our definition of γ in Eq. (37) is therefore valid for $\cos^2 \theta < 1/2$, i.e., when $\pi/4 < \theta < 3\pi/4$. From Eq. (36) we obtain

$$\gamma|_{\Delta \gg 1} = \frac{8(\Delta - a)}{\pi + 2 \arcsin(\cot^2 \theta)},$$

predicting the asymptotic slope

$$\left. \frac{\partial \gamma}{\partial \Delta} \right|_{\Delta \gg 1} = \frac{8}{\pi + 2 \arcsin(\cot^2 \theta)}. \quad (38)$$

The decay rates γ versus Δ for $Q = 0$ and fixed θ , shown in Fig. 6, play a crucial role. In what follows we demonstrate that γ for arbitrary Q is obtainable from γ for $Q = 0$ via an approximate scaling.

VII. APPROXIMATE SCALING FOR THE SHS AMPLITUDE DECAY RATE

It is tempting to generalize the convenient scaling property (26) relating expectations taken with respect to homogeneous ($Q = 0$) and nonhomogeneous ($Q \neq 0$) initial states for the $\Delta \neq 0$ regime. Simply “ignoring” the J -containing Dzyaloshinskii-Moriya (DM) term in Eq. (11) is not possible: even if in the first order in time, the DM term gives no contribution

$$\begin{aligned} e^{-iHt} |\Psi_0\rangle &\approx (I - itH' + O(t^2)) |\Psi_0\rangle \\ &= (I - itH'|_{J \rightarrow 0} + O(t^2)) |\Psi_0\rangle, \end{aligned}$$

and already for t^2 order the DM term cannot be neglected, since J and H do not commute.

However, in expansion (32) some coefficients C_k , $k \geq 2$, can become J independent, depending on the observable. In particular, one-point correlations $\langle \sigma_0^\alpha \rangle$ turn out to be J independent up to the order t^5 . For example, for $\theta = \pi/2$ we obtain

$$\begin{aligned} \langle \sigma_0^x(H, t) \rangle_Q &= 1 - \kappa(Q)t^2 + \frac{4t^4}{3} \kappa(Q) (2 \cos^2 Q + \Delta^2 \\ &\quad - \Delta \cos Q) + O(t^6), \\ \kappa(Q) &= 4(\Delta - \cos Q)^2, \end{aligned} \quad (39)$$

and the same Taylor expansion is valid for $\langle \sigma_0^x(H|_{\Delta \rightarrow \Delta/\cos Q}, t \cos Q) \rangle_0$, as can be easily checked. The equivalence of $S(Q, \Delta, t) - S(0, \frac{\Delta}{\cos Q}, t \cos Q) = O(t^6)$ means approximate overlap of the two functions at early times, and in most cases the overlapping region extends up to the time of one-half amplitude decay, as exemplified in Fig. 7. This allows to relate the half-amplitude decay rates γ of

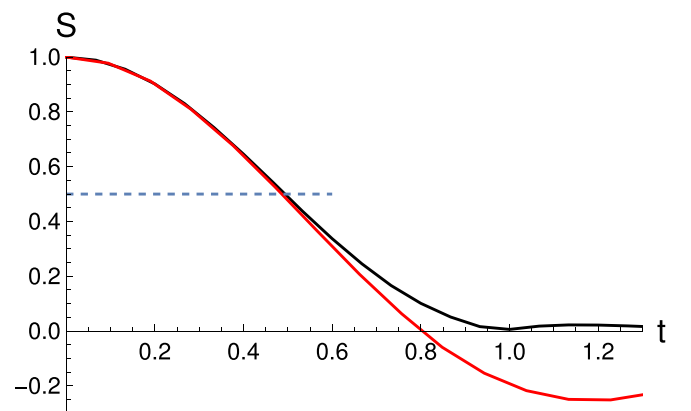


FIG. 7. Illustrating early time equivalence of $S(Q, \Delta, t)$ (black curve) and $S(0, \Delta/\cos Q, t \cos Q)$ (red curve) for $\Delta = 0.5$, $Q = 1.87$. Despite being qualitatively different at later times, the two curves overlap at early times, which allows an accurate estimate of γ from Eq. (40) at the threshold value given by crossing of $S(t)$ with the dashed line, explaining the data collapse in Fig. 8.

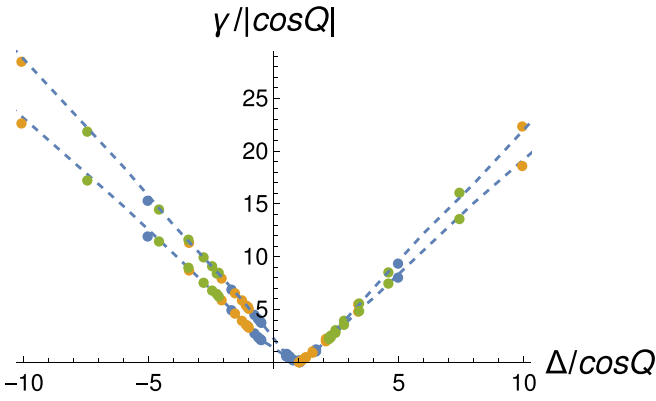


FIG. 8. Data collapse. Rescaled γ are plotted versus rescaled Δ for set of chosen parameters: $\Delta = 0.5, 1, 2.2$ (blue, yellow, and green points, respectively) and equidistant $Q = 0.07, 0.27, \dots, 3.07$, for $\theta = \pi/2$ (upper data set), $\theta = 2\pi/3$ (lower data set). Dashed curves show $\gamma(0, \Delta)$ for $Q = 0$ obtained from the points in Fig. 6 by linear interpolation.

homogeneous and nonhomogeneous SHS in an approximate way via

$$\gamma(Q, \Delta) \approx \cos Q \times \gamma\left(0, \frac{\Delta}{\cos Q}\right), \quad (40)$$

generalizing exact Eq. (27) to $\Delta \neq 0$. Technically, Eq. (40) predicts the data collapse of γ points with rescaled coordinates $\{\Delta/\cos Q, \gamma(Q, \Delta)/|\cos Q|\}$ on a single curve $\{\Delta, \gamma(0, \Delta)\}$, i.e., the curves in Fig. 6. Such a data collapse indeed exists (see Fig. 8), and it confirms the validity of Eq. (40). In addition, the approximate relation (40) becomes exact in various limits: $\Delta = 0$, $\Delta \rightarrow \cos Q$, $Q \rightarrow 0, \pi$, and also for $\Delta \gg 1$, up to Δ^{-1} corrections. Note that $\gamma(Q, \Delta)$ for some polar angle θ is related by Eq. (40) to the universal curve $\gamma(0, \Delta)$ with the same value of θ . The curve $\gamma(0, \Delta)$ at large Δ becomes a straight line with slope (38).

We conclude that the half-amplitude decay rate γ for nonzero Q can be found with good accuracy by measuring the decay rate of a homogeneous initial state with the same value of θ and a rescaled anisotropy $\Delta \rightarrow \Delta/\cos Q$, via Eq. (40).

Now we can generate the decay curves and make comparison to experimental data. By linear extrapolation of TEBD data from Fig. 6 on the full Δ axis, we obtain a set of curves $\gamma(0, \Delta)$ for different θ . From the curves $\gamma(0, \Delta)$ we generate surface $\gamma(Q, \Delta)$ (see Fig. 9) using Eq. (40), and compare a few cuts of this surface with the direct TEBD data (Fig. 10) and with the experimental data for the same quantity, called decay of contrast, in [2]. The data in Fig. 10 confirm the validity of Eq. (40), and are in qualitative accordance with the experimental data (Figs. 3(a)–3(c) in [2]) as well but there are also discrepancies worth discussing. The fit function $\gamma(Q) = \gamma_0 + \gamma_1|\Delta - \cos Q|$, used in [2] to find the anisotropy Δ , is equivalent to an approximation $\gamma = \text{const} \times (1/t_{\text{char}})$ where t_{char} is given in Eq. (35), if the offset γ_0 (due to noise) is neglected, $\gamma_0 \rightarrow 0$ (another fit function used in [2], $S(t) = 1 - \gamma t$, violates $S(t) = S(-t)$ symmetry). While for $\Delta = 0$, the approximation $\gamma \sim t_{\text{char}}^{-1}$ is exact due to Eq. (27), and is reasonable for large Δ [where γ is also large and Q -dependence can be neglected, see (36)], for $\Delta \neq 0$ and intermediate γ

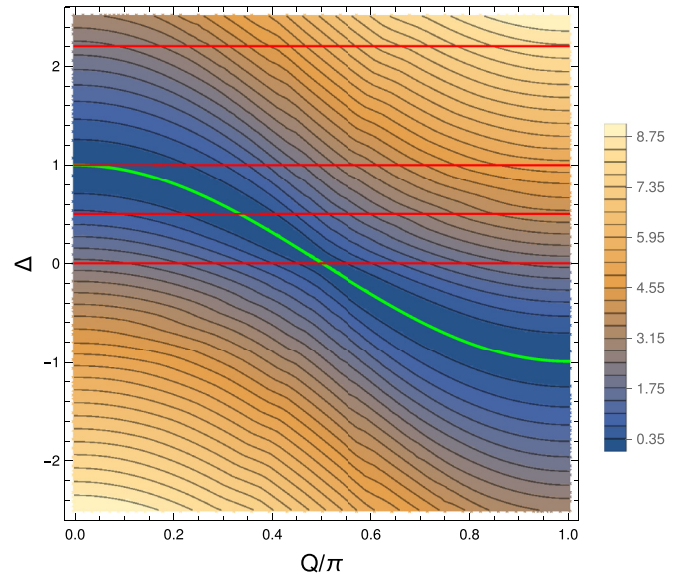


FIG. 9. Contour plot of decay rate γ versus Q/π and Δ , for $\theta = \pi/2$, obtained by using scaling relation (40). The green curve $\Delta = \cos Q$, where the SHS eigenvalue condition is met, gives the location of points with no decay, $\gamma = 0$. Cuts of the surface $\gamma(Q, \Delta)$ along the red straight lines are shown in red in Fig. 10.

values it appears rather poor (see discrepancy between dashed and solid lines in the right-hand panel of Fig. 6). A usage of scaling relation (40) with tabulated $\gamma(0, \Delta)$ appears a more promising option for the calibration of the anisotropy.

VIII. SHS: PHASE VELOCITY OF AN ASYMPTOTIC TRAVELING WAVE

Finally, we discuss the behavior of the SHS phase $\phi(t)$ in Eqs. (20) and (21). From Eqs. (23) and (24), $\phi(t)$ is an odd function of t and is nonzero only for $\theta \neq \pi/2$, and for $\Delta \neq \cos Q$. For the easy-plane regime $|\Delta| \leq 1$, $\phi(t)$ is an approximately linear function of t (see data in Fig. 11, left), thus allowing to view the SHS profile evolution as a decaying traveling wave with time-dependent phase velocity as in Fig. 1. Indeed, for linear $\phi(t)$, Eq. (20) becomes

$$\begin{aligned} \frac{\langle \sigma_n^x(t) \rangle}{\sin \theta} &= S(t) \cos(Q(n - vt) + \varphi), \\ v &= \frac{1}{Q} \frac{\partial \phi}{\partial t}. \end{aligned} \quad (41)$$

The initial phase velocity v_0 at time $t = 0$ can be estimated by a perturbative analysis (treating transversal SHS components as a perturbation; see Appendix C), yielding

$$\left. \frac{1}{Q} \frac{\partial \phi}{\partial t} \right|_{t=0} = v_0 = \frac{4(\cos Q - \Delta) \cos \theta}{Q}, \quad (42)$$

which we find in qualitative accordance with numerics (see solid lines in Fig. 12). For small θ (or $\pi - \theta$) values, the phase velocity (42) stays constant in time (see Appendix D). Generically, for $|\Delta| \leq 1$, the phase velocity $v = \phi'(t)/Q$ changes monotonically in time and quickly reaches an asymptotic value, which can be determined numerically (see open symbols in Fig. 12). On the other hand, in the easy-axis regime

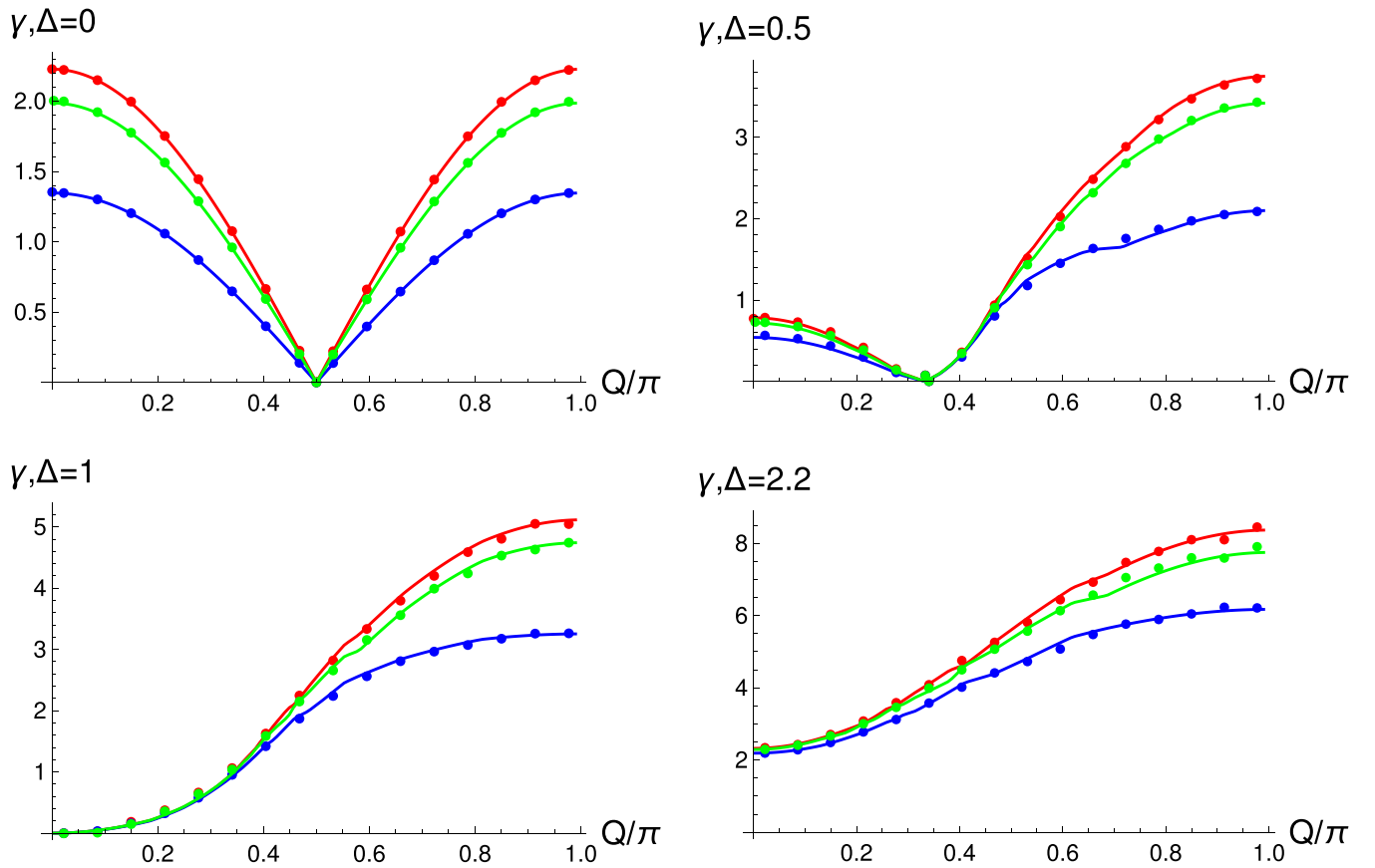


FIG. 10. Decay rate γ versus Q/π for fixed Δ , reported on the y-axis label, and selected $\theta = \frac{\pi}{2}, \frac{5\pi}{12}, \frac{2\pi}{3}$ (red, green, and blue data points, respectively). Curves with the same color code show γ calculated using the scaling relation (40) and numerical data for $Q = 0$ (like that in Fig. 6 for $\theta = \pi/2$ and $\theta = 2\pi/3$).

($|\Delta| > 1$), $\phi'(t)$ shows decaying oscillatory behavior (see right-hand panel of Fig. 11), related to the oscillatory behavior of $S(t)$ itself (see dashed curves in Fig. 4). We expect that an asymptotic phase velocity also exists in this case but it cannot be determined from TEBD because of slow convergence.

IX. TIME DEPENDENCE OF MAGNETIZATION CURRENT UNDER THE XXZ DYNAMICS

At the end, we discuss the time evolution of the SHS magnetization current $j(t) \equiv \langle j^z(t) \rangle$. Operator j^z is a $U(1)$ -invariant quantity, and therefore $j(t)$ is not expected to decay

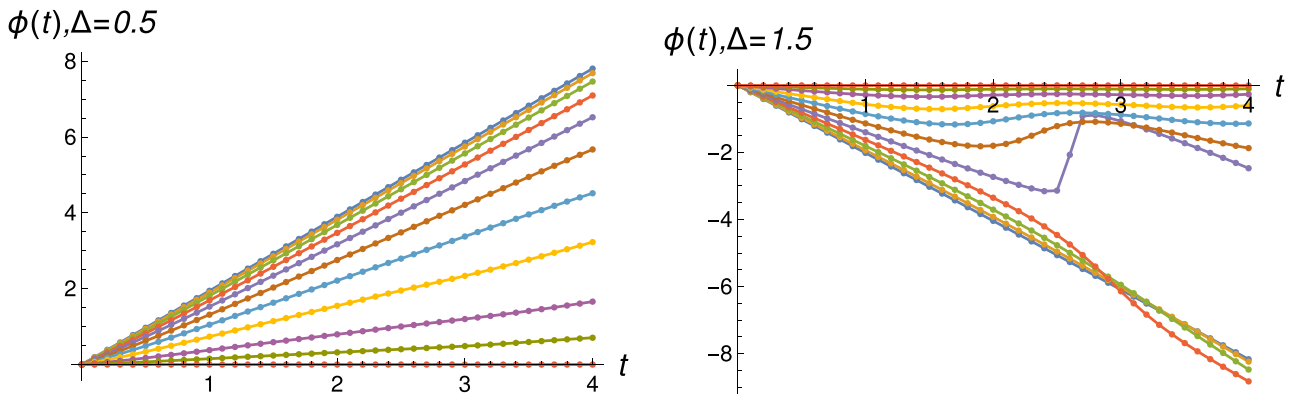


FIG. 11. Data points show phase ϕ versus time, obtained by tracking position of constant phase in the decaying SHS (see green line in Fig. 1), from TEBD calculations, for $\Delta = 0.5$ (left) and $\Delta = 1.5$ (right), for $Q = 0.14$ and different polar angles θ . Curves from top to bottom in the left panel (bottom to top in the right panel) correspond to increasing $\theta/\pi = 0.05, 0.1, 0.15, 0.2, \dots, 0.5$.

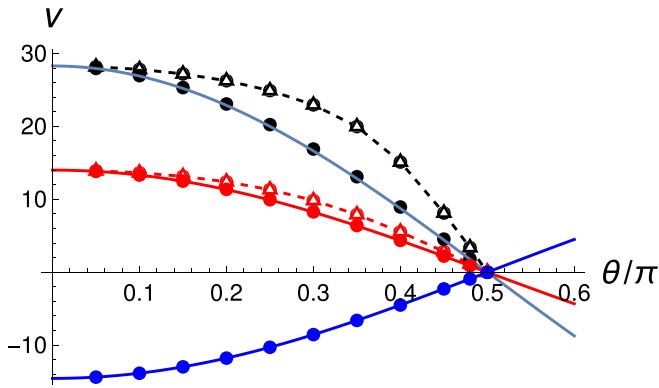


FIG. 12. Phase velocity of decaying SHS $v = \phi'(t)/Q$, for $t = 0$ (solid symbols) and $t = t_{\max}$ (open symbols), versus θ/π , obtained from the TEBD calculations, for $Q = 0.14$, and different anisotropies $\Delta = 0, 0.5, 1.5$ (black, red, and blue points, respectively). Solid lines show the prediction (42). Open symbols show the asymptotic phase velocity, determined from TEBD; the dashed lines are guides for the eye. For $\Delta = 1.5$ (the blue data) the asymptotic phase velocity cannot be determined because of oscillatory behavior (see text).

with time. From Eq. (31) we find the early time behavior

$$j(t) = j(0) - 8t^2 \Delta \sin Q (\Delta - \cos Q) \sin^4 \theta + O(t^4), \quad (43)$$

where $j(0) = 2 \sin Q \sin^2 \theta$ is the initial SHS magnetization current. From Eq. (33) the characteristic timescale for the current to change is given by

$$t_{\text{char}}(J) = |2\Delta(\Delta - \cos Q) \sin^2 \theta|^{-\frac{1}{2}}. \quad (44)$$

For $\Delta = 0$, the magnetization current is a conserved quantity, so it is time independent, which is reflected in the divergence of $t_{\text{char}}(J)$ at $\Delta = 0$.

From the TEBD, we observe that the early time behavior sets the current difference at later times, namely,

$$\begin{aligned} j^z(t > 0) - j^z(0) &> 0, & \text{if } \Delta(\cos Q - \Delta) \sin Q > 0, \\ j^z(t > 0) - j^z(0) &< 0, & \text{if } \Delta(\cos Q - \Delta) \sin Q < 0 \end{aligned} \quad (45)$$

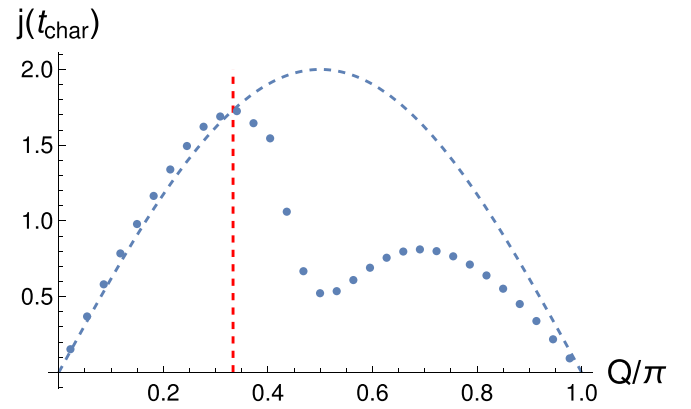
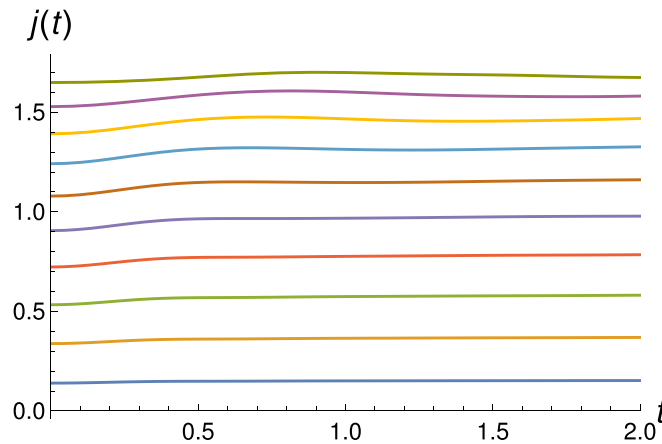


FIG. 13. Magnetization current $j(t)$ measured at time t_{char} [Eq. (44)], from TEBD (points), versus Q/π . Parameters: $\Delta = 0.5, \theta = \pi/2$. Dashed curve shows the initial SHS current $j(0) = 2 \sin Q$. Dashed vertical line at $Q = \pi/3$ corresponds to special point $\cos Q = \Delta$ for which $|\Psi_Q\rangle$ is an H eigenstate and the current stays constant in time.

(see Fig. 14 for an illustration). The TEBD data for $\Delta = 0.5$ (Fig. 13) and for other Δ values (data not shown) suggest (a) validity of Eq. (45), (b) qualitative change of behavior $j(t)$ across the eigenfunction SHS point $\cos Q = \Delta$, exemplified by the difference between the curves on the left and on the right in Fig. 14, and (c) the wave vector $Q = \pi/2$ (where the $t = 0$ SHS current is maximal) becomes a local minimum for the current value at late times.

Observations (a)–(c) deserve further study. Especially it would be interesting to see if they are valid also for the asymptotic value of the current $j(\infty)$. Unfortunately, we cannot determine $j(\infty)$ precisely enough because of the fast growth of the entanglement with time, and slow convergence. For selected parameters we tried to push the TEBD calculations as far as possible; however, the “entanglement” barrier prevents precise measurements for $t > 4$, which is not enough to see the convergence (see Fig. 15, and technical details in Appendix G).

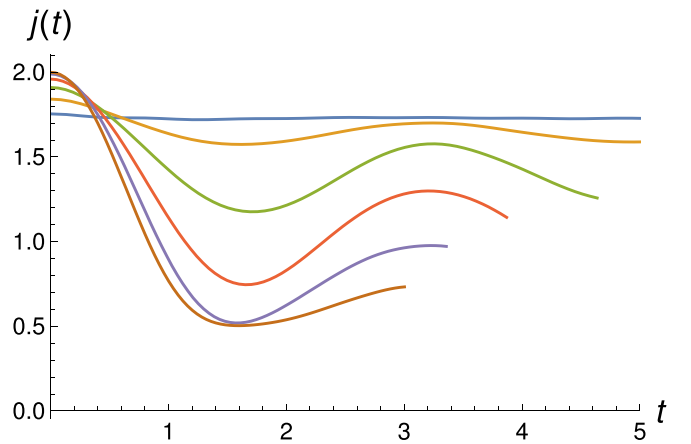


FIG. 14. Magnetization current $j(t)$, for different Q , for $\cos Q > \Delta = 0.5$ (left) and $0 \leq \cos Q \leq \Delta = 0.5$ (right), from TEBD. Parameters: left, $\theta = \pi/2, Q = 0.07, 0.17, \dots, 0.97$ (curves from bottom to top); right, $\theta = \pi/2, Q = 1.07, 1.17, \dots, 1.57 \approx \pi/2$ (curves from top to bottom at the right corner). The largest reported time for curves in the right-hand panel is given by $3t_{\text{char}}(J)$ [Eq. (44)].

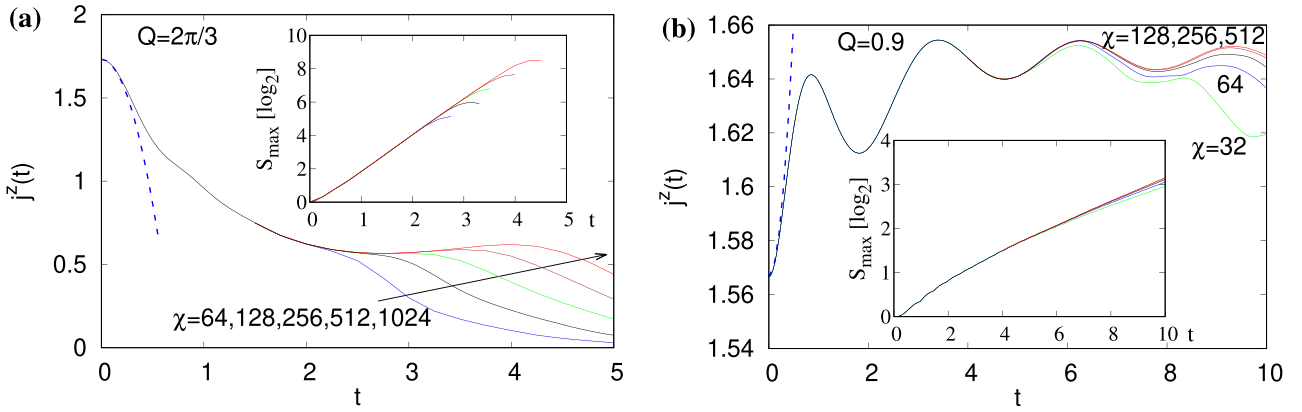


FIG. 15. Magnetization current ($j^z(t)$) versus time, from TEBD calculations with varied size χ of matrix-product state matrices in the TEBD method (see Appendix G for details). Parameters: left, $\Delta = 0.5$, $Q = 2\pi/3$, $\theta = \pi/2$; right, $\Delta = 0.5$, $Q = 0.9$, $\theta = \pi/2$. In both cases the early time behavior is well approximated by Eq. (43), indicated by dashed lines.

X. DISCUSSION

We have studied the time evolution of transversal spin helices under coherent XXZ dynamics with arbitrary z -axis anisotropy. Spin helices are chiral factorized states that can be prepared experimentally and they are of potential practical importance. We established a fundamental fact that the helix retains its harmonic space dependence at all times, which allows to describe the density profile as a traveling wave with decaying amplitude. We studied the helix profile evolution in the whole phase space via exact and approximate approaches, supported with TEBD. We found that the amplitude decay rate, the most important characteristic from a practical viewpoint, satisfies the scaling relation, relating decay of homogeneous ($Q = 0$) and inhomogeneous ($Q \neq 0$) setups. The scaling relation allows to obtain the decay rate of a transversal helix with arbitrary wavelength in a system with arbitrary anisotropy from a single scaling function. At the free-fermion point, the scaling relation holds for all quantum observables. Furthermore, we studied how the current of magnetization evolves in time. We proposed a criterion for the asymptotic current and pointed out open problems of interest for further investigations. We expect that our findings are of direct interest for experimentalists and can serve for calibration purposes in future experiments.

ACKNOWLEDGMENTS

V.P. acknowledges financial support by the European Research Council through the advanced Grant No. 694544-OMNES, from the Deutsche Forschungsgemeinschaft through DFG project KL 645/20-2 (V.P.), and Slovenian Research Agency, Program P1-0402 and J1-4385 (M.Z.). X.Z. acknowledges the financial support from the National Natural Science Foundation of China (Grant No. 12204519).

APPENDIX A: SHS DECAY: TIME ASYMPTOTIC FORM IN THE THERMODYNAMIC LIMIT $N \rightarrow \infty$

Under usual generic assumptions (the eigenstate thermalization hypothesis), a $U(1)$ -invariant operator like H on an infinite lattice, acting on a generic state, imposes the $U(1)$

symmetry on any finite subsystem asymptotically in time, making the asymptotic reduced density matrix of the subsystem commute with the generator of $U(1)$, namely,

$$\lim_{t \rightarrow \infty} \lim_{N \rightarrow \infty} [\rho_{n_1 n_2 \dots n_M}(t), \sigma_{n_1}^z \cdots \sigma_{n_M}^z] = 0, \quad \forall M, \{n_k\} \quad (\text{A1})$$

(note that the limits $t \rightarrow \infty$ and $N \rightarrow \infty$ do not commute), where $\sigma_{n_1}^z \cdots \sigma_{n_M}^z$ is the generator of the $U(1)$ symmetry $U_z = \bigotimes_n \sigma_n^z$ restricted to the subsystem. In terms of averages (5), Eq. (A1) yields

$$\lim_{t \rightarrow \infty} \lim_{N \rightarrow \infty} \langle \sigma_{n_1}^{\alpha_1} \sigma_{n_2}^{\alpha_2} \cdots \sigma_{n_k}^{\alpha_k}(t) \rangle = 0, \quad \text{if } m_+ \neq m_-, \quad (\text{A2})$$

where $\alpha_j = +, -, z$ and m_+ (m_-) is the total number of pluses (+) (minuses $-$) in the upper row of indices in Eq. (A2). Indeed only the operators $\sigma_{n_1}^{\alpha_1} \sigma_{n_2}^{\alpha_2} \cdots \sigma_{n_k}^{\alpha_k}$ with $m_+ = m_-$ commute with U_z . For one- and two-point correlations we have

$$\lim_{t \rightarrow \infty} \lim_{N \rightarrow \infty} \langle \sigma_n^\pm(t) \rangle = 0, \quad \forall n, \quad (\text{A3})$$

$$\lim_{t \rightarrow \infty} \lim_{N \rightarrow \infty} \{ \langle \sigma_n^\pm \sigma_m^\pm(t) \rangle, \langle \sigma_n^+ \sigma_m^+(t) \rangle, \langle \sigma_n^- \sigma_m^-(t) \rangle \} = 0, \quad \forall n, m. \quad (\text{A4})$$

Consequently, the reduced density matrices for one and two sites written in the computational basis, asymptotically in time become block diagonal:

$$\lim_{t \rightarrow \infty} \lim_{N \rightarrow \infty} \rho_n(t) = \frac{1}{2} \begin{pmatrix} a & 0 \\ 0 & d \end{pmatrix}, \quad \forall n, \quad (\text{A5})$$

$$\lim_{t \rightarrow \infty} \lim_{N \rightarrow \infty} \rho_{n,m}(t) = \begin{pmatrix} a & 0 & 0 & 0 \\ 0 & b & b_1 & 0 \\ 0 & b_1^* & c & 0 \\ 0 & 0 & 0 & d \end{pmatrix}, \quad \forall n, m. \quad (\text{A6})$$

The generic form of the asymptotic-in-time reduced density matrix for arbitrary sites M is block diagonal as in Eq. (A6), and satisfies Eq. (A1).

APPENDIX B: SYMMETRIES OF SHS AMPLITUDE AND PHASE $S_N(Q, \theta, \Delta, t)$ AND $\phi(Q, \theta, \Delta, t)$

Consider operator $U_x = \bigotimes_{n=-\infty}^{\infty} \sigma_n^x$, and the operator R of mirror reflection with respect to the middle site 0 which has the property

$$U_x |\Psi_{Q,\theta}\rangle = |\Psi_{-Q,\pi-\theta}\rangle, \quad (\text{B1})$$

$$R |\Psi_{Q,\theta}\rangle = |\Psi_{-Q,\theta}\rangle, \quad (\text{B2})$$

where θ is the polar angle characterizing the SHS. Using the properties $[H, U_x] = 0$, $R^\dagger = R$, $U_x^\dagger = U_x$, we obtain

$$\langle A \rangle_{Q,\pi-\theta} = \langle U_x A U_x \rangle_{-Q,\theta}, \quad (\text{B3})$$

$$\langle A \rangle_{-Q} = \langle R A R \rangle_Q. \quad (\text{B4})$$

Here and below we use the shorthand notations $\langle A \rangle_{Q,\theta}$, $\langle A \rangle_{Q,\varphi}$, $\langle A \rangle_Q$ to denote generic expectation of an operator A : $\langle A(H, t) \rangle_{Q,\theta,\varphi} = \langle \Psi_{Q,\theta,\varphi} | e^{iHt} A e^{-iHt} | \Psi_{Q,\theta,\varphi} \rangle$ (e.g., using $\langle A \rangle_Q$ means that θ and φ are the same on both sides of an equality).

In particular, for one-point correlations we obtain

$$\langle \sigma_n^x \rangle_{Q,\pi-\theta} = \langle \sigma_n^x \rangle_{-Q,\theta}, \quad (\text{B5})$$

$$\langle \sigma_n^{y,z} \rangle_{Q,\pi-\theta} = -\langle \sigma_n^{y,z} \rangle_{-Q,\theta}, \quad (\text{B6})$$

$$\langle \sigma_0^\alpha \rangle_{-Q} = \langle \sigma_0^\alpha \rangle_Q, \quad \alpha = x, y, z, \quad (\text{B7})$$

the last one following from $R \sigma_0^\alpha R = \sigma_0^\alpha$, since mirror reflection R does not touch the central site.

Comparing an identity $\langle \sigma_n^+ \rangle_{\pi-\theta} = \langle R \sigma_n^- R \rangle_\theta = \langle \sigma_{-n}^- \rangle_\theta$ and comparing to Eqs. (20) and (21), we obtain

$$S_N(\pi - \theta) = S_N(\theta), \quad \phi(\pi - \theta) = -\phi(\theta). \quad (\text{B8})$$

Analogously, analyzing the identity $\langle \sigma_n^+ \rangle_Q = \langle R \sigma_n^+ R \rangle_{-Q} = \langle \sigma_{-n}^+ \rangle_{-Q}$,

$$S_N(Q) = S_N(-Q), \quad \phi(Q) = \phi(-Q). \quad (\text{B9})$$

Since $\langle \sigma_n^x(t) \rangle_{Q,\varphi}$ is a real number, we obtain

$$\begin{aligned} \langle \sigma_n^x(t) \rangle_{Q,\varphi} &= \langle \Psi_{Q,\varphi} | e^{iHt} \sigma_n^x e^{-iHt} | \Psi_{Q,\varphi} \rangle \\ &= \langle \Psi_{-Q,-\varphi} | e^{-iHt} \sigma_n^x e^{iHt} | \Psi_{-Q,-\varphi} \rangle \\ &= \langle \sigma_n^x(-t) \rangle_{-Q,-\varphi}. \end{aligned} \quad (\text{B10})$$

With the help of Eqs. (B9), one can prove

$$S_N(Q, t) = S_N(-Q, t) = S_N(Q, -t), \quad (\text{B11})$$

$$\phi(Q, t) = \phi(-Q, t) = -\phi(Q, -t). \quad (\text{B12})$$

For an even N , if Q satisfies Eq. (3), $\pi \pm Q$ satisfies Eq. (3) as well. Using Eq. (9), one can prove that when $Q \rightarrow Q + \pi$

$$\begin{aligned} H' |_{Q \rightarrow Q+\pi} &= -H' |_{\Delta \rightarrow -\Delta}, \\ (\sigma_n^\pm)' |_{Q \rightarrow Q+\pi} &= e^{\pm i\pi n} (\sigma_n^\pm)', \\ \langle \sigma_n^\pm(H, t) \rangle_{Q+\pi} &= e^{\pm i\pi n} \langle \sigma_n^\pm(H |_{\Delta \rightarrow -\Delta}, -t) \rangle_Q, \end{aligned}$$

which leads to the relations

$$\begin{aligned} S_N(Q, \Delta, t) &= S_N(-Q, \Delta, t) = S_N(\pi - Q, -\Delta, -t) \\ &= S_N(\pi - Q, -\Delta, t), \end{aligned} \quad (\text{B13})$$

$$\begin{aligned} \phi(Q, \Delta, t) &= \phi(-Q, \Delta, t) = \phi(\pi - Q, -\Delta, -t) \\ &= -\phi(\pi - Q, -\Delta, t). \end{aligned} \quad (\text{B14})$$

Selected relations of this Appendix are quoted in the text, omitting the repeated symbols for brevity.

APPENDIX C: PROOF OF EQUATION (42)

Consider a time evolution of a density matrix in the form of a homogeneous diagonal factorized state perturbed by a nondiagonal term with wave vector Q :

$$\begin{aligned} \rho_\epsilon(0) &= R^{\otimes N} + \epsilon \sum_n A_n, \\ A_n &= R^{\otimes n-1} \otimes F_n \otimes R^{\otimes N-n}, \\ R &= \begin{pmatrix} a & 0 \\ 0 & d \end{pmatrix}, \quad a = \frac{1}{2} + \frac{\cos \theta}{2}, \quad d = 1 - a, \\ F_n &= \begin{pmatrix} 0 & e^{-iQn} \\ e^{iQn} & 0 \end{pmatrix}. \end{aligned} \quad (\text{C1})$$

The time-evolved state is

$$\begin{aligned} \rho_\epsilon(t) &= \rho_\epsilon(0) - it[H, \rho_\epsilon(0)] - \frac{t^2}{2} ad_H^2 \rho_\epsilon(0) + \dots \\ &= \rho_\epsilon(0) - i\epsilon t \sum_n [h_{n,n+1}, A_n + A_{n+1}] + O(t^2) \\ &= \rho_\epsilon(0) - i\epsilon t \sum_n R^{\otimes n-1} \\ &\quad \otimes [h, F_n \otimes R + R \otimes F_{n+1}] \otimes R^{\otimes N-n-1} + O(t^2), \end{aligned} \quad (\text{C2})$$

where $h = \sigma^x \otimes \sigma^x + \sigma^y \otimes \sigma^y + \Delta(\sigma^z \otimes \sigma^z - I)$ is the energy density of the Hamiltonian H and we used $[h, R \otimes R] = 0$. Denoting

$$X' = \sigma^z X, \quad (\text{C3})$$

and substituting easily verifiable relations

$$\begin{aligned} [h, F \otimes R] &= 2\Delta(F' \otimes R') - 2(R' \otimes F'), \\ [h, R \otimes F] &= 2\Delta(R' \otimes F') - 2(F' \otimes R'), \end{aligned}$$

into Eq. (C2), we readily obtain

$$\begin{aligned} \rho_\epsilon(t) &= \rho_\epsilon(0) - i\epsilon t \sum_n Z_{n,n+1} + O(t^2), \\ Z_{n,n+1} &= 2R^{\otimes n-1} \otimes (\Delta F'_n \otimes R' \\ &\quad - R' \otimes F'_n + \Delta R' \otimes F'_{n+1} - F'_{n+1} \otimes R') \otimes R^{\otimes N-n-1}. \end{aligned} \quad (\text{C4})$$

Let us now calculate the observable $\langle \sigma_n^+(t) \rangle$ using Eq. (C4):

$$\langle \sigma_n^+(t) \rangle = \langle \sigma_n^+(0) \rangle - i\epsilon t \sum_{m=n-1}^n \text{tr}(Z_{m,m+1} \sigma_n^+) + O(t^2). \quad (\text{C5})$$

Substituting

$$\begin{aligned} \text{tr}(Z_{n-1,n} \sigma_n^+) &= 2\text{tr}((-F'_{n-1} + \Delta F'_n) \sigma_n^+) \text{tr}(R R') \\ &= 2(e^{iQ(n-1)} - \Delta e^{iQn}) \cos \theta, \end{aligned} \quad (\text{C6})$$

$$\text{tr}(Z_{n,n+1} \sigma_n^+) = 2(-\Delta e^{iQn} + e^{iQ(n+1)}) \cos \theta, \quad (\text{C7})$$

into Eq. (C5) we finally obtain

$$\begin{aligned} \langle \sigma_n^+(t) \rangle &= \epsilon e^{iQn} (1 - 2it(e^{iQ} + e^{-iQ} - 2\Delta) \cos \theta) + O(t^2) \\ &\approx \epsilon e^{iQn} e^{-4it(\cos Q - \Delta) \cos \theta} \\ &= \epsilon e^{i(Qn - \phi(t))} = \epsilon e^{i(Q(n - v_0 t))}, \end{aligned} \quad (\text{C8})$$

$$v_0 = \frac{4(\cos Q - \Delta) \cos \theta}{Q}, \quad (\text{C9})$$

where v_0 is the phase velocity of the infinitesimal perturbations. Quite remarkably, our rather simple analysis turns out to predict qualitatively correctly the initial phase velocity $v_0 = \phi'(0)/Q$, even though the Q -dependent amplitude is not infinitesimally small (see Fig. 12 of the main text).

APPENDIX D: $S_N(t)$ AND $\phi(t)$ FOR $\theta \rightarrow 0$ CASE

$|\Psi_{Q,\theta,\varphi}\rangle$ is a linear combination of $N + 1$ independent states $|\xi_0\rangle, |\xi_1\rangle, \dots, |\xi_N\rangle$ [12]:

$$|\Psi_{Q,\theta,\varphi}\rangle = e^{-\frac{i}{2}(N\varphi + Q \sum_{n=0}^{N-1} n)} \cos^{\frac{N}{2}} \frac{\theta}{2} \sum_{m=0}^N \tan^{\frac{m}{2}} \frac{\theta}{2} e^{im\varphi} |\xi_m\rangle, \quad (\text{D1})$$

$$|\xi_m\rangle = \sum_{k_1 < k_2 < \dots < k_m} e^{iQ \sum_{j=1}^m k_j} \sigma_{k_1}^- \dots \sigma_{k_m}^- |\uparrow \uparrow \dots \uparrow\rangle. \quad (\text{D2})$$

In the $\theta \rightarrow 0$ limit, $\tan \frac{\theta}{2} \rightarrow 0$; therefore, we only consider the first two leading terms, i.e., $|\xi_0\rangle$ and $|\xi_1\rangle$. Since $e^{iNQ} = 1$, one can prove that both $|\xi_0\rangle$ and $|\xi_1\rangle$ are eigenstates of H :

$$H |\xi_1\rangle = 4(\cos Q - \Delta) |\xi_1\rangle, \quad H |\xi_0\rangle = 0. \quad (\text{D3})$$

Then, we have

$$\begin{aligned} \langle \sigma_n^x(t) \rangle &= \langle \Psi_{Q,\theta,\varphi} | e^{iHt} \sigma_n^x e^{-iHt} | \Psi_{Q,\theta,\varphi} \rangle \\ &= \cos^{2N} \frac{\theta}{2} \left(\langle \xi_0 | + \tan \frac{\theta}{2} e^{-i\varphi + 4i(\cos Q - \Delta)t} \langle \xi_1 | \right) \\ &\quad \times \sigma_n^x \left(|\xi_0\rangle + \tan \frac{\theta}{2} e^{i\varphi - 4i(\cos Q - \Delta)t} |\xi_1\rangle \right) + \dots \\ &= \cos^{2N} \frac{\theta}{2} \tan \frac{\theta}{2} \left(e^{i\varphi - 4i(\cos Q - \Delta)t} \langle \xi_0 | \sigma_n^x |\xi_1\rangle \right. \\ &\quad \left. + e^{-i\varphi + 4i(\cos Q - \Delta)t} \langle \xi_1 | \sigma_n^x |\xi_0\rangle \right) + \dots \\ &= 2 \cos^{2N} \frac{\theta}{2} \tan \frac{\theta}{2} \cos(nQ - 4t(\cos Q - \Delta) + \varphi) \\ &\quad + \dots, \end{aligned} \quad (\text{D4})$$

$$\begin{aligned} \langle \sigma_n^y(t) \rangle &= \langle \Psi_{Q,\theta,\varphi} | e^{iHt} \sigma_n^y e^{-iHt} | \Psi_{Q,\theta,\varphi} \rangle \\ &= \cos^{2N} \frac{\theta}{2} \left(\langle \xi_0 | + \tan \frac{\theta}{2} e^{-i\varphi + 4i(\cos Q - \Delta)t} \langle \xi_1 | \right) \\ &\quad \times \sigma_n^y \left(|\xi_0\rangle + \tan \frac{\theta}{2} e^{i\varphi - 4i(\cos Q - \Delta)t} |\xi_1\rangle \right) + \dots \\ &= \cos^{2N} \frac{\theta}{2} \tan \frac{\theta}{2} \left(e^{i\varphi - 4i(\cos Q - \Delta)t} \langle \xi_0 | \sigma_n^y |\xi_1\rangle \right. \\ &\quad \left. + e^{-i\varphi + 4i(\cos Q - \Delta)t} \langle \xi_1 | \sigma_n^y |\xi_0\rangle \right) + \dots \\ &= 2 \cos^{2N} \frac{\theta}{2} \tan \frac{\theta}{2} \sin(nQ - 4t(\cos Q - \Delta) + \varphi) \\ &\quad + \dots, \end{aligned} \quad (\text{D5})$$

which leads to the following asymptotic behavior in the limit $\theta \rightarrow 0$:

$$\lim_{\theta \rightarrow 0} \frac{\langle \sigma_n^x(t) \rangle}{\sin \theta} = \cos(nQ - 4t(\cos Q - \Delta) + \varphi), \quad (\text{D6})$$

$$\lim_{\theta \rightarrow 0} \frac{\langle \sigma_n^y(t) \rangle}{\sin \theta} = \sin(nQ - 4t(\cos Q - \Delta) + \varphi), \quad (\text{D7})$$

$$\lim_{\theta \rightarrow 0} S_N(t) = 1, \quad (\text{D8})$$

$$\lim_{\theta \rightarrow 0} \phi(t) = 4t(\cos Q - \Delta). \quad (\text{D9})$$

APPENDIX E: ISING CASE

Here we find the SHS amplitude time dependence, for the $\Delta \gg 1$ limit. The rescaled amplitude S_N is given by

$$S_N(t) = \frac{2}{\sin \theta} \sqrt{\langle \sigma_0^+(t) \rangle \langle \sigma_0^-(t) \rangle}. \quad (\text{E1})$$

For large $\Delta \gg 1$, in the zero-order approximation, we neglect the hopping part of the Hamiltonian,

$$\langle \sigma_0^+(t) \rangle = \langle \Psi_Q | e^{iH_{00z}t} \sigma_0^+ e^{-iH_{00z}t} | \Psi_Q \rangle, \quad (\text{E2})$$

where $H_{00z} = \Delta \sum_{n=0}^{N-1} \sigma_n^z \sigma_{n+1}^z$. Using $|\Psi_Q\rangle = U_Q |\Psi_0\rangle$, with $U_Q = e^{-i\frac{Q}{2} \sum_{n=0}^{N-1} n \sigma_n^z}$ we obtain, using the diagonality of H_{00z} , and $[U, \sigma_0^\alpha] = 0$,

$$\begin{aligned} \langle \Psi_Q | e^{iH_{00z}t} \sigma_0^+ e^{-iH_{00z}t} | \Psi_Q \rangle &= \langle \Psi_0 | U_Q^\dagger e^{iH_{00z}t} \sigma_0^+ e^{-iH_{00z}t} U_Q | \Psi_0 \rangle \\ &= \langle \Psi_0 | e^{iH_{00z}t} \sigma_0^+ e^{-iH_{00z}t} | \Psi_0 \rangle \\ &= \langle \Psi_0 | V_{N-1,0}^\dagger V_{01}^\dagger \sigma_0^+ V_{01} V_{N-1,0} | \Psi_0 \rangle, \quad V_{n,m} = e^{-i\Delta t \sigma_n^z \sigma_m^z}. \end{aligned}$$

After straightforward calculation involving three qubits located at consecutive positions $N - 1, 0, 1$, we obtain

$$\langle \sigma_0^+(t) \rangle = \frac{1}{8} e^{i\varphi - 4i\Delta t} \sin \theta [1 - \cos \theta + (1 + \cos \theta) e^{4i\Delta t}]^2. \quad (\text{E3})$$

Complex conjugation of the above gives $\langle \sigma_0^-(t) \rangle$. Substituting in Eq. (E1), after some algebra we obtain

$$S_N(t) = \frac{1}{2} [1 + \cos^2 \theta + \sin^2 \theta \cos(4\Delta t)]. \quad (\text{E4})$$

This describes harmonic motion with a positive nonzero mean. Note that there is no dependence on the wavelength Q . For fixed $\theta \neq \pi/2$ (SHS out of the XY plane), the amplitude stays always positive,

$$\min_t S_N(t) = \cos^2 \theta. \quad (\text{E5})$$

The presence of the small hopping term in the Hamiltonian, neglected in our calculation, for large but finite Δ leads to (a) slow gradual decrease of the amplitude $S(t)$ in accordance with the $U(1)$ symmetry restoration principle [Eq. (A5)], and (b) to $1/\Delta$ corrections to Eq. (E4), which can be incorporated into a finite shift of Δ value in Eq. (E4). For $Q = 0$, $\theta = \pi/2$ we found $\Delta \rightarrow \Delta - 1.3$ effective shift by a comparison to numerical data for large Δ (data not shown).

APPENDIX F: TAYLOR EXPANSION FOR $N \rightarrow \infty$

The operator expansion

$$e^X A e^{-X} = A + [X, A] + \frac{1}{2!} [X, [X, A]] + \dots = \sum_{n=0}^{\infty} \frac{1}{n!} ad_X^n(A), \quad (\text{F1})$$

$$ad_X(A) = [X, A], \quad ad_X^0(A) = A, \quad (\text{F2})$$

with X substituted by iHt and A being the operator of a chosen observable, allows to find Taylor expansions, up to certain order, for any observable in the thermodynamic limit.

From Eq. (31), substituting $X \rightarrow iHt$, we obtain

$$\langle A(t) \rangle = \langle A(0) \rangle + \sum_{k>0} C_k t^k. \quad (\text{F3})$$

To determine the C_k in Eq. (F3), we embed the operator A close to site $n = 0$ and calculate the term by using symbolic

$S^2(\theta, t)$

$$\begin{aligned} &= 1 + 8 \sin^2 \theta \left(-t^2 + \frac{t^4}{3} (3 \cos(2\theta) + 17) - \frac{2t^6}{45} (156 \cos(2\theta) + 5 \cos(4\theta) + 511) + \frac{t^8}{315} (6777 \cos(2\theta) + 758 \cos(4\theta)) \right. \\ &+ 7 \cos(6\theta) + 19914) - \frac{2t^{10}}{14175} (256792 \cos(2\theta) + 68804 \cos(4\theta) + 2792 \cos(6\theta) + 11 \cos(8\theta) + 916529) \\ &+ \left. \frac{2t^{12}}{467775} (5602870 \cos(2\theta) + 5557480 \cos(4\theta) + 460051 \cos(6\theta) + 11410 \cos(8\theta) + 55 \cos(10\theta) + 48757510) \right) + O(t^{14}), \end{aligned} \quad (\text{F6})$$

(further terms of the expansions are too bulky to be reported).

With this method we obtain all the other Taylor expansions in the thermodynamic limit quoted in the main text. Note that, as usual, the Taylor expansion (F3) has a finite radius of convergence.

APPENDIX G: NUMERICAL TIME EVOLUTION

To evolve the initial SHS state $|\Psi_Q\rangle$ with unitary propagator $U(t) = e^{-iHt}$ we write the state in the matrix-product state (MPS) form

$$|\Psi_Q\rangle = \sum_s c_s |s\rangle, \quad c_{s=s_1, \dots, s_N} = \langle 1 | M_1^{(s_1)} M_2^{(s_2)} \dots M_N^{(s_N)} | 1 \rangle, \quad (\text{G1})$$

in terms of two matrices M_j^s of size $\chi \times \chi$ for each site j , and use the standard TEBD method [21]. In brief, we split the nearest-neighbor $H = A + B$ into noncommuting A and B , each acting on even and odd pairs of spins, respectively. Time evolution is split into small time steps of length dt , for which we then Trotterize the propagator into terms involving only A , or only B , each involving commuting nearest-neighbor transformations. While higher-order Trotter-Suzuki schemes are advantageous, we here use a simple leapfrog scheme, $U(dt) \approx e^{-iAdt/2} e^{-iBdt} e^{-iAdt/2}$. Applying one nearest-neighbor unitary transformation acting on

calculations (*Mathematica*)

$$C_k = \langle \Psi_{Q, \theta, \varphi} | \frac{1}{k!} ad_{iH}^k(A) | \Psi_{Q, \theta, \varphi} \rangle, \quad (\text{F4})$$

where $|\Psi_{Q, \theta, \varphi}\rangle$ is defined in Eq. (2) and Q satisfies Eq. (3). The system size N must be chosen sufficiently large to exclude the finite-size effects. For an operator A embedded on a cluster of sites $n \in [-f, f]$, $[H, A]$ is embedded on a cluster $n \in [-f-1, f+1]$, and $ad_{iH}^k(A)$ is embedded on a cluster $n \in [-f-k, f+k] = [-n_L, n_R]$. To guarantee the absence of finite-size effects, the cluster $[-n_L, n_R]$ must lie entirely inside the segment $[-\frac{N}{2}, \frac{N}{2}]$, i.e.,

$$\frac{N}{2} - 1 \geq n_R, \quad -\frac{N}{2} \leq -n_L. \quad (\text{F5})$$

For one-point correlations embedded on site $n = 0$, $n_L = n_R = k$, and we have $N \geq 2(k+1)$ from Eq. (F5).

Finally, for products of observables $\langle A \rangle \langle B \rangle$, a further resummation of the Taylor expansion must be made. The Taylor expansion of the amplitude $S^2(t) = \frac{4}{\sin^2 \theta} \langle \sigma_0^+ \rangle \langle \sigma_0^- \rangle$ for $Q = \Delta = 0$ thus obtained is

sites j and $j+1$ mixes the MPS form on those two sites, which is then restored after doing a singular value decomposition. The time complexity of simulating one unit of time (that consists of $\sim 1/dt$ leapfrog steps) scales as $\sim \chi^3 n/dt$, while the error due to the leapfrog scheme scales as $\sim (dt)^2$. Keeping the MPS representation exact would require the bond size χ to be equal to the rank of the reduced density operator. Because that rank quickly grows in t , and soon saturates at its maximal value that is exponential in N , one needs to truncate matrices to some fixed maximal size χ . How large truncation errors due to this finite χ are then depends on the spectrum of the reduced density matrix. Roughly speaking one can estimate the required χ to be exponential in the von Neumann entropy. Because von Neumann entropy will generically grow linearly in time this means that the maximal reliable time up to which we can simulate unitary evolution scales as $\ln \chi$; even for $\chi \sim 10^3$ this is rather small.

As an example, in Fig. 15(a) we have an example where the prefactor in the linear growth of von Neumann entropy is large: one has $S(t=3) \approx 6$ and $S(t=4) \approx 8$, meaning, e.g., that with $\chi = 256$ one can simulate up to $t \approx 3$, with $\chi = 1024$ only up to $t \approx 4$. Increasing χ from 256 to 1024 increases CPU time by $\approx 4^3 = 64$ while bringing in only one additional unit of time. If entanglement is smaller, an example would be $Q = 0.9$ in Fig. 15(b), one can go to

longer times and get more precise results; however, ultimately one again runs into an “entanglement” barrier where no further simulation in time is feasible. We also note that in Fig. 15(a) where the current varies a lot we could use

Trotter time step $dt = 0.05$, while in Fig. 15(b), where the current changes much less on the shown time $t \approx 10$, we wanted the errors to be much less than 1%, and we had to use $dt = 0.01$.

-
- [1] S. Hild, T. Fukuhara, P. Schauß, J. Zeiher, M. Knap, E. Demler, I. Bloch, and C. Gross, *Phys. Rev. Lett.* **113**, 147205 (2014).
 - [2] P. N. Jepsen, Y. K. Lee, H. Lin, I. Dimitrova, Y. Margalit, W. W. Ho, and W. Ketterle, *Nat. Phys.* **18**, 899 (2022).
 - [3] P. N. Jepsen, J. Amato-Grill, I. Dimitrova, W. W. Ho, E. Demler, and W. Ketterle, *Nature (London)* **588**, 403 (2020).
 - [4] P. N. Jepsen, W. W. Ho, J. Amato-Grill, I. Dimitrova, E. Demler, and W. Ketterle, *Phys. Rev. X* **11**, 041054 (2021).
 - [5] J. F. Rodriguez-Nieva, A. P. Orioli, and J. Marino, *Proc. Natl. Acad. Sci. USA* **119**, e2122599119 (2022).
 - [6] C. Psaroudaki and C. Panagopoulos, *Phys. Rev. Lett.* **127**, 067201 (2021).
 - [7] S. Kühn, F. Gerken, T. H. Lena Funcke, P. Stornati, K. Jansen, and T. Posske, [arXiv:2302.02603](https://arxiv.org/abs/2302.02603).
 - [8] E. S. Ma, K. L. Zhang, and Z. Song, *Phys. Rev. B* **106**, 245122 (2022).
 - [9] T. Posske and M. Thorwart, *Phys. Rev. Lett.* **122**, 097204 (2019).
 - [10] V. Popkov and C. Presilla, *Phys. Rev. A* **93**, 022111 (2016).
 - [11] V. Popkov and G. M. Schuetz, *Phys. Rev. E* **95**, 042128 (2017).
 - [12] V. Popkov, X. Zhang, and A. Klümper, *Phys. Rev. B* **104**, L081410 (2021).
 - [13] D. Pereira and E. J. Mueller, *Phys. Rev. A* **106**, 043306 (2022).
 - [14] G. Cecile, S. Gopalakrishnan, R. Vasseur, and J. De Nardis, [arXiv:2211.03725](https://arxiv.org/abs/2211.03725).
 - [15] S. Moudgalya, B. A. Bernevig, and N. Regnault, *Rep. Prog. Phys.* **85**, 086501 (2022).
 - [16] X. Zhang, A. Klümper, and V. Popkov, *Phys. Rev. B* **103**, 115435 (2021).
 - [17] I. E. Dzyaloshinskii, *Sov. Phys. JETP* **19**, 960 (1964).
 - [18] T. Moriya, *Phys. Rev.* **120**, 91 (1960).
 - [19] V. Popkov, X. Zhang, and A. Klümper, [arXiv:2303.14056](https://arxiv.org/abs/2303.14056).
 - [20] R. Durrett, *Probability: Theory and Examples*, Vol. 49 (Cambridge University Press, Cambridge, U.K., 2019).
 - [21] U. Schollwöck, *Ann. Phys.* **326**, 96 (2011).